INNOVATIVE LIPIDIC NANOCARRIERS OF FLUTAMIDE ENHANCING ITS *IN VITRO* CYTOTOXICITY AND *IN VIVO* ORAL BIOAVAILABILITY: DESIGN, OPTIMIZATION, CHARACTERIZATION, AND PHARMACOKINETIC ASPECTS

MOHAMED A. ALI[1], MAGDY I. MOHAMED[2*], KHALID M. EL-SAY[3], MOHAMED A. MEGAHED[4]

[1,2]Department of Pharmaceutics and Industrial Pharmacy, Faculty of Pharmacy, Cairo University, Cairo, Egypt. [3]Department of Pharmaceutics, Faculty of Pharmacy, King Abdulaziz University, Jeddah-21589, Saudi Arabia. [4]Department of Pharmaceutics and Pharmaceutical Technology, Egyptian Russian University, Cairo, Egypt
*Corresponding author: Magdy I. Mohamed; *Email: mohamed@pharma.cu.edu.eg

ABSTRACT

Objective: the reduced oral bioavailability of Flutamide has hindered its effectiveness as a chemotherapeutic agent for prostate cancer treatment. Our study aimed to enhance FLUTAMIDE *in vitro* cytotoxicity and oral bioavailability *via* its incorporation into lipid nanocarriers that contained solid lipid (Precirol®) alone or in combination with anti-androgenic oils such as Saw Palmetto Oil (SPO) and Pumpkin Seed Oil (PSO).

Methods: we employed the Box Behnken Design (BBD) to optimize Flutamide-loaded nanocarriers, focusing on mean vesicular size, zeta potential, and entrapment efficiency.

Results: the optimized nanovesicles exhibited dimensions of 330.2 nm, a zeta potential of -43.1 mV, and an entrapment efficiency of 66.1%. Morphological analysis using Transition Electron Microscope (TEM) and Scanning Electron Microscope (SEM) confirmed the spherical shape of the nanovesicles. Differntial Scanning Calorimetry (DSC) thermograms and X-ray diffractograms indicated decreased crystallinity of encapsulated Flutamide compared to free Flutamide. *In vitro* cytotoxicity studies demonstrated enhanced effects against prostate cancer cells (PC-3) for optimized Flutamide-loaded nanocarriers containing the 2 anti-androgenic oils over both nanocarriers containing no oils and free Flutamide suspension. *In vivo* pharmacokinetic analysis in male rats showed increased oral bioavailability for flutamide-loaded nanocarriers with C_{max} values of 559.35±41.79 ng/ml and 670.9±24.61 ng/ml for different formulations compared to the free flutamide suspension with a C_{max} value of 281.4±94.33 ng/ml.

Conclusion: These findings support FLUTAMIDE oral bioavailability improvement through nanocarriers encapsulation, advocating its utilization in prostate cancer therapy and approving the additive anti-androgenic effect after its combination with SPO and PSO.

Keywords: Bioavailability, Box-behnken design, Flutamide, PC-3 cell line, MTT assay, Optimization, Pharmacokinetic

INTRODUCTION

Benign Prostatic Enlargement (BPE) is described as a hypertrophy of both epithelial and stromal cells in the prostate gland transitional zone that leads toward the expansion of the prostate gland [1]. The related pathophysiologic mechanisms in the progress of BPE and its advanced state Prostate Carcinoma (PCa) include age-correlated enhanced 5α-reductase conversion of testosterone into the highly active DiHydroTestosterone (DHT) that lead to unrestrained proliferation of the prostate gland cells through their action on androgenic receptors [2, 3]. In the management guidelines of hormone-responsive neoplasms like the prostatic one, androgen receptor antagonists like flutamide (flutamide) are thought to play a generous role [4].

FLUTAMIDE is a first-generation non-steroidal anti-androgenic agent taken orally for treating both BPE and progressive PCa. Similarly, it acts on androgen receptors, competitively blocking the interaction of both testosterone and dihydrotestosterone with the receptors [5]. In accordance with the Biopharmaceutical Classification System (BCS), flutamide is considered a class II drug with slight solubility in water and, therefore, reduced wettability [3, 6]. Accordingly, an innovative flutamide-containing carrier is mandatory to ① enhance solubility, permeability, and escape first hepatic metabolism, therefore improving bioavailability via increasing drug concentration at absorption sites; ② target flutamide exclusively to the prostatic tissue without causing harm to other organs [7–9]. Additionally, combining flutamide with herbal remedies may add value to the outcomes by decreasing the dose of flutamide needed and lowering the potential for adverse effects [10]. Patients have access to a wide range of herbal treatments for this indication. They most frequently contain phytosterols, lectins, and β-sitosterol as their active ingredients. Two widespread herbal treatments are PSO and SPO [11].

The Cucurbitaceae family includes the pumpkin (Cucurbita pepo species) [10, 12]. PSO has been consumed in traditional European medicine to treat BPE alone or in conjugation with saw palmetto due to the inhibitory effect of the 5-alpha reductase enzyme that participates in the formation of DHT from testosterone in the prostatic tissue, which has a major enlarging effect on the tissues. Accordingly, it can be concluded that PSO might be a new therapeutic option for treating BPE [10, 12, 13].

Notwithstanding the established contribution of PSO in BPE, the species Serenoa contains one genus, *Serenoa repens*, often known as saw Palmetto oil or SPO, a part of the Arecaceae palm tree that originates on the southern coast of the USA [2, 13]. SPO used as a treatment for BPE symptoms due to anti-androgenic effect *via* blocking the formation of DHT that is considered the potent metabolite of testosterone through inhibition of 5-alpha reductase enzyme and also prevent binding DHT with its androgenic receptors [14, 15].

Lipid-based NanoParticles (LNPs) are among the most popular nano-transporters and have several benefits due to their low toxicity, excellent compatibility with biological systems, and controlled drug release profiles [16-19]. lNPs can be employed to successfully enhance the solubility, stability, and safety of several medications being incorporated into them [20]. Solid lipid Nanoparticles (SLNs), Nanostructured lipid Carriers (NLCs), lipid nano-capsules, and other lNPs have all been used recently in research [21]. Solid lipids make up the majority of SLNs, such as high-melting-point glycerides or waxes, which replace the liquid

lipids used in emulsions. SLN is regarded as the first generation of lipid nano-transporters; their matrix can tightly bind drugs, prevent their degradation, and achieve controlled drug release. However, they continue to have some drawbacks, including restrictions on drug loading capacity and drug expulsion during storage. As a result, the NLC, a new and improved generation of lipid NPs, was developed [16, 22–24].

NLCs are thought to be an evolution of the original SLNs because of their unique structure, which preserves solid lipids from being recrystallized and, therefore, provides a more stable system on the thermodynamic level that improves drug accommodation to boost drug packing capacity and prevent its ejection. Three categories of NLCs have been described: (I) imperfect type, (II) amorphous type, and (III) multiple type [23, 25].

In forming lNPs, such as SLNs, NLCs, and other drug cargo systems, experimental designs are considered an efficient and potent tool because they make it possible to examine many variables at once in a few number of experimental runs [26, 27]. Response surface approach is widely used, greatly replacing the tedious one-factor-at-a-time approach. Based on a collection of mathematical and statistical techniques, it simulates and analyzes formulation problems [28, 29]. This method's primary goal is to optimize the response surface affected by different process factors and determine the relationship between the acquired response surfaces and the adjustable input parameters [28]. BBD is one of the response surface designs that is a 2nd order rotatable or nearly rotatable based on a three-level incomplete factorial design that can be used for investigating quadratic response surfaces and also produces a 2nd degree polynomial model that can be utilized to optimize a process with a limited number of trials by decreasing the number of experimental runs. BBD not only spares time but also saves the experiments' cost [30, 31].

This study aims to formulate different types of enhanced stable flutamide-loaded lipid nanotransporters; one with spatially varied solid lipid only (Precirol®) and the other using solid lipid in addition to two different liquid lipids having enhanced BPE activity (PSO and SPO) for enhancing the solubility, and therefore the bioavailability of

flutamide against prostate cancer using BBD for optimization of the different process parameters.

MATERIALS AND METHODS

Materials

Flutamide was kindly donated to us by Sigma for Pharmaceutical Industries (Qwesna, Egypt). Precirol ATO5® was kindly donated as a gift sample from Gattefosse (Saint-Priest, France). Saw palmetto oil was gifted to us by Jamjoom Pharmaceuticals Co. (Jeddah, Saudi Arabia). Pumpkin seed oil was purchased from Imtenan for nutritional and healthy products (Cairo, Egypt). Chloroform HPLC was purchased from Central Drug House ltd. (New Delhi, India). Absolute HPLC Methyl alcohol was acquired from VWR International (Paris, France). Dimethyl sulfoxide, 3-(4, 5-dimethylthiazol-2-yl)-2, and 5-diphenyltetrazolium bromide salt (MTT) were obtained from Sigma-Aldrich Company (St. louis, MO, USA). Potassium phosphate dibasic anhydrous, Tween 20, and soya lecithin were obtained from loba Chemie (Mumbai, India). Orthophosphoric acid was purchased from Piochem (Cairo, Egypt).

Design of experiment

A 3^3-BBD was used to optimize different variables in formulation of FLUTAMIDE-loaded nanocarriers (NCs). Three independent variables are selected to be liquid lipid percentage from total lipid (X_1), Surface Active Agent (SAA) concentration (X_2), and lecithin concentration (X_3) to investigate their outcome on the designated dependent variables. Our objectives are to minimize mean vesicular size (Y_1) while maximizing both the Zeta Potential (ZP) (Y_2) and entrapment efficiency (Y_3). A description of the different variables, with their levels, and the designated responses are revealed in table 1. A total of 15 experimental trials were generated with triplicate center points. According to BBD, the components of the generated flutamide-loaded nanocarriers are revealed in table 2. ANOVA was used as a statistical test to analyze the significance of factors, effects, and interactions between them *via* Statgraphics® Centurion XV software, version 15.2.05, (StatPoint, Inc., Warrenton, VA, USA), where the mathematical relations were elucidated as polynomial equations.

Table 1: Dependent and independent variables of BBD of flutamide-loaded nanocarrier

Independent variables (Factors)	Levels			Units
	Low (-1)	Medium (0)	High (+1)	
X_1: liquid lipid percentage from total lipid	0	15	30	%
X_2: Surfactant concentration	0.5	1	1.5	%
X_3: lecithin concentration	0	50	100	mg
Dependent variables (Responses)	Units		Goal	
Y_1: mean particle size	nm		Minimize	
Y_2: Zeta potential	mV		Maximize	
Y_3: Entrapment efficiency	%		Maximize	

Preparation of flutamide-loaded nanocarriers

The hot emulsification-sonication method was employed to prepare flutamide-loaded and blank nanocarriers [19, 32]. A total amount of lipid, including both solid and liquid lipids, is chosen to be 390 mg, of which the liquid lipid ratio may be (0, 15, or 30%, i. e., 0, 58.5, or 117 mg/formula); the liquid lipid is added in a ratio (1:1) of both SPO and PSO. The drug is added in a fixed amount (10 mg/formula) to all 15 formulations. The lipids, lecithin, and flutamide are adequately dissolved in 30 ml of a mixture of chloroform and methanol (1:1) in a 250 ml round bottom flask. Organic solvents were then entirely evaporated using a rotary vacuum evaporator, Büchi-M/HB-140 (Flawil, St. Gallen, Switzerland), run at 50 rpm for 25 minutes to produce a drug-embedded-lipid thin layer. Then, the drug-loaded lipid layer was melted in a water bath heated to 75 °C. The aqueous phase consisted of 10 ml of tween 20 solution (prepared by dissolving tween 20 according to each conc. in double-distilled water) and heated to the same temperature as molten lipids, then added dropwise to the melted lipids with continuous stirring at 3000 rpm and a temperature maintained at 75 °C. Finally, the

produced suspension was sonicated at 75 °C for 5 minutes at 20 kHz and refrigerated at 8°C. Each formulation was prepared by changing the experiment factors, as shown in table 2, and the blank of each formula was also prepared using the same method but without adding the drug.

Characterization of flutamide-loaded nanocarriers

Entrapment efficiency % determination

The entrapment efficiency percentage was determined using the direct method. The un-entrapped flutamide was separated from 1 ml of the formulated suspension via centrifugation using a cooling centrifuge (Centurion Scientific ltd., Stoughton, UK) for 2 h at a temperature of around 4 °C with a force of 15,000×g. Then, the supernatant was discarded, and a washing cycle was applied in order to ensure that there was no longer free flutamide in the gaps between the particles via rinsing the pellets with double-distilled water, then re-centrifuged again after being redispersed with a vortex mixer. After that, in order to release the drug that had been trapped, the residue was ruptured by adding a 1:1 mixture of

methanol and chloroform, then sonicated until a clear solution was obtained, which was then detected spectrophotometrically at wavelength 302 nm using a Jasco V-630, UV-visible spectrophotometer (Tokyo, Japan) [9]. A drug-free nanocarrier was treated with the same technique and used as a blank in the measurement. EE% was done as follows: [33, 34].

$$EE\% = \frac{\text{Amount of entrapped flutamide}}{\text{Total amount of flutamide added in the formulation}} \times 100 \dots \text{(Eq. 1)}$$

Measurement of the mean vesicular size and particle surface charge

All formulations (F_1-F_{15}) were diluted 15 times with double-distilled water before being measured, then subjected to a probe sonicator for one minute to eradicate air and fragment any clumps of particles [27, 32]. Then, using a Dynamic laser light Scattering (DLS) on a Zetasizer Nano ZS (Malvern Instruments, UK), the PolyDispersity Index (PDI), particle's surface charge (mV), and mean nanoparticle diameter (nm) of flutamide-loaded nanocarrier for all formulations were determined at 25 °C with a scattering angle of 90°.

Prediction, preparation, and assessment of the optimal formula

BBD was successfully applied using Statgraphics software, and the trials were created by choosing the input factors with their suitable levels. After the multifarious response optimization, the optimized flutamide formula was predicted based on the obtained results for each response (Y_1–Y_3). It was then prepared and evaluated three times for each response (Y_1–Y_3) to ensure that the predicted and measured Optimized Formula (OF) responses were authentic. Additionally, another formula was prepared with the same amounts of the optimized formula but Without addition of liquid lipids (WL) to assess if there are any additive effect of the PSO and SPO when they have been combined with flutamide.

Transmission electron microscopy

Utilizing a transmission electron microscope (Jeol: JEM-2100, Tokyo, Japan), it was possible to measure the NCs size precisely and distinguish between OF and WL *via* visualization of their morphologic structures. To enable a flawless assessment of the generated NCs, both OF and WL were diluted significantly with double-distilled water to an appropriate strength. Then one drop of the diluted suspension was put on a grid coated in carbon (C_{12}) and allowed to sit for a minute to allow some of the particles to adhere to it. The extra dispersion was then wiped away with a piece of filter paper. Then the sample was smeared with one drop of 1% phosphotungstic acid solution, and any excess was removed with filter paper. The material was allowed to dry in the air before being examined under an electron microscope [35, 36].

Lyophilization and physical characterization of flutamide-loaded nanocarriers

Aqueous dispersions of OF and WL nanocarriers were iced overnight in a freezer at an ultra-low temperature of-80°C (WUF-25, Daihan Scientific Co., ltd., Korea). Then, a lab freeze-dryer (Christ Alpha 2-4 lSC Basic, Germany) was utilized to lyophilize the samples using mannitol as cryoprotectant. The freeze-drying was conducted for 24 h.

Morphological study

Droplets of undiluted OF were applied on an aluminum specimen stub, and the sample was then allowed to dry overnight. Then the Sample was gold sputtered for 5 min before examination and then imaged by a scanning electron microscope (ZEISS-EVO 15, UK) run at an accelerating voltage of 25 kV to explore the surface structure of lyophilized OF [28].

Differential scanning calorimetry (DSC)

Differential scanning calorimetry model DSC 6 (PerkinElmer, USA) was used to record thermograms of Precirol ATO5, lecithin, FLUTAMIDE, and also their physical mixture, OF, and WL to scrutinize the physical state of FLUTAMIDE inside the lyophilized NCs as well as observe its compatibility with the other formulation components. Samples (around 3 mg) were subjected to heating in a temperature range of 30-300 °C at 10 °C per min in a nitrogen

environment with a flow rate of 20 ml per minute in locked aluminum pots with a similar vacant pan was used as a reference. The instrument was occasionally standardized with indium [19, 37].

X-ray diffraction (XRD) analysis

A modern diffractometer (Bruker, D8 Advance, Germany) with Cu Kα_1 radiation (λ = 1.54060) at 40 kV and 40 mA between 5° and 80° (2θ) at room temperature, with a step size of 0.05° and a scan speed of 1°/min, was used to detect X-ray diffractograms for pure flutamide, lyophilized OF, and lyophilized WL [19].

Cell culture and cytotoxicity assay (MTT)

Cancer cells from two distinct cell lines (PC-3 and VERO) were bought from the American Type Culture Collection (Manassas, VA, USA) and grown up on Roswell Park Memorial Institute medium (RPMI 1640) enriched with 1% of 0.1 g/ml streptomycin, 0.1 units/µl of penicillin, and 10% of heat-deactivated fetal bovine serum in a moistened, 5% (v/v) CO_2 atmosphere at 37 °C. Then, cells from the two cell lines were subjected to exponential proliferation and then treated with the trypsin enzyme to detach adherent cells from the vessel in which they were being cultured; after that, they were counted and distributed into ninety-six well microtiter plates with a density of five thousand cells/0.33 cm^2 of well. At that time, cells were incubated for one day in a humid atmosphere at 37 °C to develop a complete monolayer sheet. Subsequently, cells were subjected to varying concentrations (0.1, 10, 100, and 1000 µM) of the three formulas: OF, WL, and Free Flutamide Suspension (FDS) for two successive days to detect the viability of treated cells *via* MTT technique as follows: after decantation of the excess media from 96-well microtiter plates, 0.2 ml 5% MTT solution (Sigma Aldrich, MO, USA) was added per well to the cells for incubation, then the cells are permitted to convert the dye into a colorful, formazan crystal (insoluble) for four hours, subsequently discarding the leftover MTT solution from each well, 0.2 ml of DMSO per well was used to dissolve the formazan crystals. Finally, *via* an Epoch-2c plate reader (Biotek, Winooski, VT, USA), absorbance was measured at 570 nm. GraphPad Prism version 10 software (Graph Pad Software Inc., San Diego, CA, USA) was used to calculate the Concentration that causes 50% Inhibition of cell proliferation (IC_{50}) and to express the cell viability as a percentage of control [38, 39]. The IC_{50} values of different groups were compared statistically using a Statistical Package for Social Sciences (SPSS) software using a one-way Analysis Of Variance (ANOVA) followed by Tukey's range test, as shown in table 4.

In vivo pharmacokinetic study on male rats

protocol

The *in vivo* pharmacokinetic study was conducted in compliance with the protocol approved by the Cairo University Faculty of Pharmacy's Animal Ethical Committee (PI 3107), using male Sprague-Dawley rats weighing an average of 300±25 g. The rats were housed at normal conditions of temperature, humidity, and light (12 h of light/dark alternations) in cages made of plastic with a mesh cover that allow free access to standard laboratory diet and water. The rats were allocated into three groups of six (groups I, II, and III) and given a single oral dose of 26 mg/kg of OF, WL, and FDS, respectively, following a one-night fast from food and unrestricted access to water [9]. Glycerin and 0.2% gum tragacanth were combined with deionized water to prepare a free flutamide suspension [26].

Samples collection and storage

Using K-EDTA-containing tubes (VACUTECH, Egypt), blood was withdrawn from the rat's retro-orbital plexus in samples of 0.5 ml each at predefined periods (0, 15, 30, 60, 120, 240, 360, and 480 minutes). The plasma was then separated through centrifugation of the collected blood at 5000 rpm for 15 min using a cooling centrifuge (Centurion Scientific ltd., Stoughton, UK), followed by their storage at-80 °C using an ultra-low-temperature freezer (WUF-25, Daihan Scientific Co., ltd., Korea) until further High Performance liquid Chromatography (HPLC) analysis using the modified HPLC method previously described [9, 37, 40].

Plasma samples treatment and HPLC assay

A constant amount of plasma (0.25 ml) was treated with the addition of methyl alcohol in a ratio of 1:2 to precipitate the soluble plasma proteins before injecting the supernatant into the HPLC column. After adding methanol, the solution is mixed in a vortex mixer (Paramix II, Julabo labortechnik GmbH, Seelbak, Germany) for one minute followed by centrifugation at 10,000 rpm for twenty minutes. Finally, 0.1 ml of the clear supernatant was introduced onto HPLC column RP-18, a 250 x 4.6 mm column (Xterra, Milford, MA, USA) of the HPLC apparatus (Waters Alliance 2695, Milford, MA, USA) equipped with a Photo Diodo Array (PDA) detector for assaying the exact amount of flutamide in each sample. The entire run and retention times were approximately 8 and 6.5 minutes, respectively, at 302 nm using a mobile phase involving methanol and water in a ratio of 70:30 (v/v) at a flow rate of 1 ml/min. A calibration curve was constructed by plotting the peak area against concentration, which produces a linear relation with $R^2 > 0.9996$ over the concentration range of 100–4000 ng/ml. Utilizing the non-compartmental method of analysis, PK Solver software was used to calculate the different parameters.

RESULTS AND DISCUSSION

Design of experiment (BBD) then optimization of flutamide-loaded nanocarriers via response surface methodology (RSM)

Based on literature and preliminary studies, the main factors affecting NLC formulation are: ① solid lipid (Precirol ATO5®)because of the highly porous structural properties that formed via mono-, di-, and triglyceride esters (mainly diglycerides) of palmitic and stearic acids which facilitate better drug accommodation and improve its solubility [41]; ② liquid lipids; selected to SPO and PSO due to their significance effect in the management of BPE [10]; ③ surfactant; tween 20 is chosen due to its greater solubility improvement effect on flutamide [7]; and ④ co-surfactant; lecithin is chosen because of a good particle stabilizing properties [42, 43]. 15 flutamide-loaded formulations have been prepared in our study in accordance with BBD recommendations. Flutamide was successfully incorporated into lipid NTs as a drug cargo to improve its solubility and oral bioavailability. The BBD is considered one of the popular experimental designs that is suitable for investigating quadratic response surfaces and generates a second-degree multinomial model, which in turn is used in optimizing a process using a small number of experimental runs in comparison to other experimental designs that, by applying the same number of factors and levels (3^3) give a larger number of runs, e. g., the central composite design gives a total number of 16 runs while the 3^3-Factorial design gives 27 runs.

Using Statgraphics software and a two-way ANOVA test, multiple regression analysis is used to statistically examine the BBD obtained data. Table 3, presents the evaluated factor effects and corresponding *p*-values for each of the three factors. A positive sign denotes a synergistic result, which is a direct relationship between the factor effect and the response. Conversely, an antagonistic outcome is indicated by a negative sign (inverse link between the factor effect and the examined response). A *p*-value of less than 0.05 indicates a significant factor, interaction, or quadratic effect. Also, Pareto charts and main effect plots in fig. 1 and 2 confirmed the association between the factors and respnses and their significance. Furthermore, the 3D plots (response surface) in fig. 3 showed the effect of all factors on the responses over the designated levels of factors.

Table 2: Composition of BBD formulations of flutamide-loaded nanocarriers and their acquired responses (Y_1-Y_3), and the predicted and observed responses of the optimized formula

Run	X_1 (%)	X_2 (%)	X_3 (mg)	Y_1 (nm)	Y_2 (-mV)	Y_3 (%)
1	15	1	50	252.8	33.5	62.9
2	0	1	0	296.5	27.7	77.3
3	30	0.5	50	279.6	34.8	58.9
4	30	1.5	50	229.9	33.3	50.8
5	15	1	50	259.1	34.6	62.4
6	15	1.5	100	242.3	35.8	57
7	30	1	0	219.9	31	60
8	30	1	100	250.6	35.9	62.7
9	15	1	50	255.1	32.9	65.3
10	0	0.5	50	325.8	25.4	74.2
11	15	0.5	100	273.3	30.5	61.9
12	15	1.5	0	130.1	24.4	58.7
13	15	0.5	0	216.2	23.3	71.4
14	0	1	100	402.1	28	55
15	0	1.5	50	233.5	24.3	53.3
Predicted optimized formula	29.2	1.17	100	268.6	38.4	62.1
95% C. I				204.7 – 332.6	32.2 – 44.7	56 – 68.2
Observed optimized formula				330.2	43.1	66.1

Table 3: Statistical ANOVA results of the responses (Y_1-Y_3)

Responses	Y_1		Y_2		Y_3	
Factors	Effect	*p*-value	Effect	*p*-value	Effect	*p*-value
X_1	-69.475	0.0195*	7.4	0.0144*	-6.85	0.0173*
X_2	-64.775	0.0252*	0.95	0.6569	-11.65	0.0019*
X_3	76.4	0.0136*	5.95	0.0317*	-7.7	0.0110*
X_1^2	88.3333	0.0328*	-2.06667	0.5167	-2.73333	0.3861
X_1X_2	21.3	0.4958	-0.2	0.9467	6.4	0.0686
X_1X_3	-37.45	0.2532	2.3	0.4559	12.5	0.0063*
X_2^2	-65.2667	0.0830	-6.36667	0.0844	-5.73333	0.1031
X_2X_3	27.55	0.3859	2.1	0.4939	3.9	0.2177
X_3^2	-15.1167	0.6379	-3.96667	0.2384	3.16667	0.3216
R^2 (%)	91.3825		85.6607		95.1119	
Adj-R^2 (%)	75.8711		59.8499		86.3134	
SEE	29.0097		2.84734		2.76683	
MAE	13.4444		1.31778		1.27556	

Note: *significantly differs at a *P*-value<0.05.

Estimation of the quantitative effects of the factors, interactions, and quadratic effects

Effects on the mean vesicular size (Y$_1$)

The mean vesicular size of all formulations (Y$_1$) ranged from 130.1 nm for F12 to 402.1 nm for F14. The polydispersity index (PDI) of all formulations ranged from 0.264 for F2 to 0.466 for F6, which indicates a uniform allocation of vesicular size. The obtained data indicated that the primary component responsible for the variation in the mean vesicular diameter of flutamide-loaded NCs, as depicted in fig. 1 and 2, was the lecithin conc. (X$_3$). It was noted that X$_3$ has a significant direct association with the vesicular size (Y$_1$) with a *p*-value of 0.0136. An instance of the lecithin influence on the vesicular size was the increase in size observed in F11 (273.3 nm) after addition of 100 mg lecithin to fixed levels of both X$_1$ and X$_2$ as compared to F13 (216.2 nm) and in F14 (402.1 nm) after addition of 100 mg lecithin to the same levels of both X$_1$ and X$_2$ in comparison with F2 (296.5 nm). This finding could be attributed to the fact that when the concentration of stabilizer rises, soy lecithin deposits onto lipid vesicles, increasing vesicular size, a finding previously reported in several studies [28, 44-46]. The second factor significantly affecting the mean vesicular size with a *p*-value of 0.0195 was the liquid lipids percentage to total lipid (X$_1$), which has an inverse relationship with the vesicle size. An increase in the liquid lipids percentage from 0 to 30% reduces Y$_1$ from 402.1 nm to 250.6 nm for F14 and F8, respectively, and from 325.8 nm to 279.6 for F10 and F3, respectively. The reduction of vesicular size could be explained by the expulsion of liquid lipid that occurs during NLC preparation as soon as solid lipid recrystallizes when the system cools down, where the liquid lipid may still be present outside or dispersed at random due to its soft structure [47]. Finally, the last factor that significantly impacted the vesicular size was tween 20 concentration (X$_2$), which significantly affected the size at a *p*-value of 0.0252. As noted from table 2, keeping factors X$_1$ and X$_3$ constant with increasing tween 20 concentration from 0.5% in F3 with a vesicular size of 279.6 nm to 1.5% will decrease the size of F4 to 229.9 nm. The same finding was found in F11, with a size of 273.3 nm, which was reduced to 242.3 nm in F6, and F13, with a size of 216.2 nm, reduced to 130.1 nm in F12. The increments in surface active agent concentration will reduce surface tension and free energy at the vesicular surface generated during due to high shearing stress, leading to a drop in particle size. This conclusion is consistent with earlier research [41, 43]. Also, the quadratic effect of X$_1$ was found to inversely affect the vesicular size with a significant *p*-value of 0.0328. The quadratic model equation that explains the effects of the independent variables on vesicular size was:

$$Y_1 = 253.179 - 8.37639\ X_1 + 147.442\ X_2 + 0.889833\ X_3 + 0.196296\ X_1^2 + 1.42\ X_1X_2 - 0.0249667\ X_1X_3 - 130.533\ X_2^2 + 0.551\ X_2X_3 - 0.00302333\ X_3^2 \ldots \text{(Eq. 2)}$$
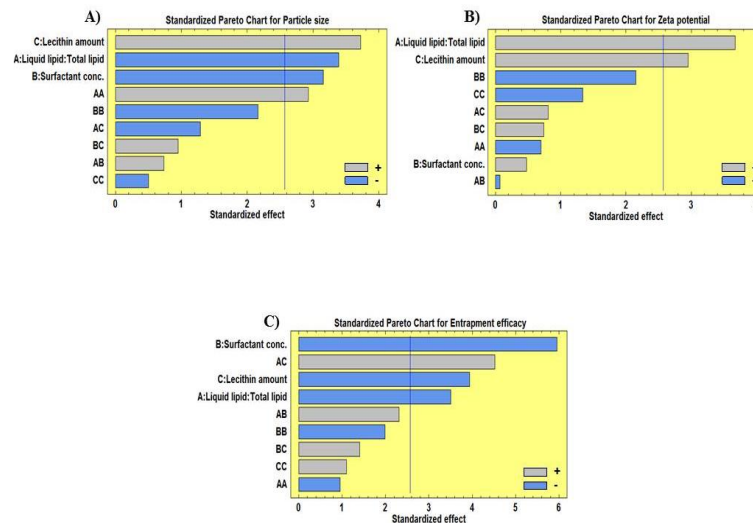

Fig. 1: Pareto charts revealing the effects of independent variables (X$_1$ – X$_3$) on (A) Particle size, (B) Zeta potential, and (C) Entrapment efficacy
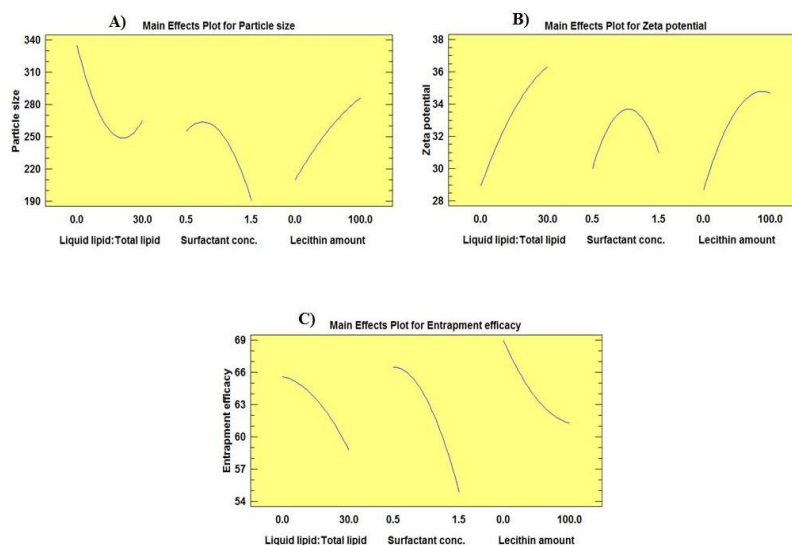

Fig. 2: Main effect plots showing the effects of different factors (X$_1$ – X$_3$) on (A) Particle size, (B) Zeta potential, and (C) Entrapment efficacy
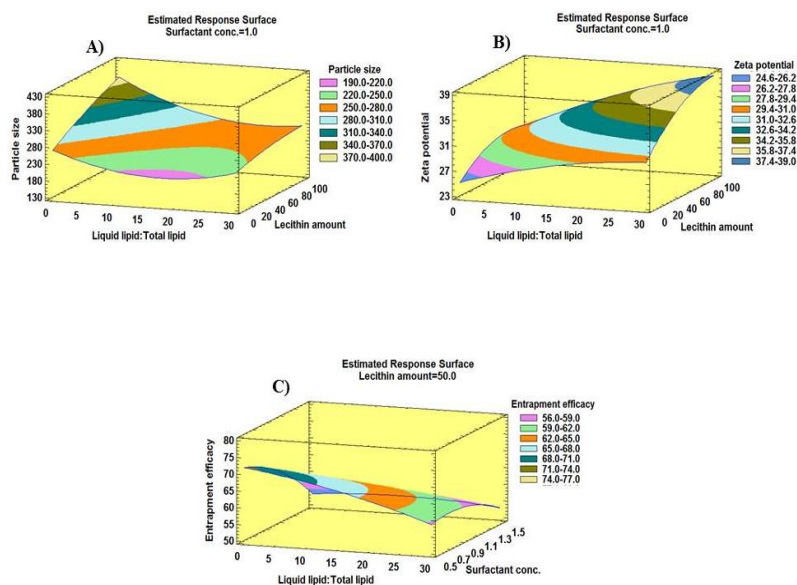
Fig. 3: Expected response surfaces with three-dimensional contour plots illustrating the influence of investigated factors (X_1 – X_3) on (A) Particle size, (B) Zeta potential, and (C) Entrapment efficacy

Effects on zeta (ζ) potential (Y_2)

ZP is considered the electro-kinetic potential that controls the stability of colloidal systems, including SLNs and NLCs. It measures the repulsion between particles that prevents their aggregation during storage. The electro-kinetic potential of all formulations (Y_2) ranged from-23.3 mV for F13 to-35.9 mV for F8, as displayed in fig. 1 and 2. of liquid lipid percentage to total lipid (X_1) was the most substantial factor that directly influences the ζ potential of FLUTAMIDE-loaded NCs, with a *p*-value of 0.0144. For illustration, as noted in table 2, the ZP for F2, F10, F14, and F15 that don't include any amount of liquid lipids in their composition were-27.7,-25.4,-28, and-24.3 mV, respectively. These values increased dramatically in the corresponding formulas that have the same composition except for the addition of 30% of SPO and PSO to be-31,-34.8,-35.9, and-33.3 mV for F7, F3, F8, and F4, respectively (increasing the value while disregarding the negative sign). The reason behind that finding may be due to the high free fatty acid content of both oils (oleic, lauric, myristic, and palmitic acids) that lead to the buildup of negatively charged ionized carboxyl groups (-COO⁻) on the surface of the particles, a finding that is consistent with several previous studies containing oleic acid as the liquid portion for the preparation of NLC [48, 49]. Furthermore, the lecithin amount added to the formula (X_3) was established to have a significant synergistic effect on ZP (Y_2) with a *p*-value of 0.0317, which can be confirmed *via* noting the increase in ZP for F6, F8, F11, and F14 to-35.8,-35.9,-30.5, and-28 mV, respectively, after the addition of 100 mg of lecithin to the corresponding formulas, F12 (-24.4 mV), F7 (-31 mV), F13 (-23.3 mV), and F2 (-27.7 mV), that were made of the same ingredients but containing no lecithin. The effect of lecithin on ZP can be credited to the ionic properties of the phosphatidylcholine-containing co-surfactants in the lipid matrix, which impart a negative charge to the nanoparticles they contain [50]. The quadratic model equation describing the relation between several variables and ZP:

Y_2 = 13.3417+0.321111 X_1+24.5167 X_2+0.0738333 X_3-0.00459259 X_1^2-0.0133333 X_1X_2+0.00153333 X_1X_3-12.7333 X_2^2+0.042 X_2X_3-0.000793333 X_3^2 (Eq. 3)

Effects on the EE% (Y_3)

The entrapment efficiency of all preparations (Y_3) ranged from 50.8% for F4 to 77.3% for F2, as revealed in table 2 and fig. 1-3. The major factor indirectly proportionate with the EE% was tween 20 conc. (X_2) with a *p*-value of 0.0019, an effect may be attributed to several theories, for example, an increase in SAA concentration is thought to reduce the vesicular size of NCs, which reduces the amount of space available for FLUTAMIDE and increases its escape into the surrounding aqueous medium, thereby lowering the EE% [10] and also, the partition phenomenon could explain this decline in EE%. A high level of surfactant in the external phase promotes the drug's solubilization in this phase, increasing the drug's partition from the internal to the external phase [51]. That effect can be demonstrated via observation in table 2, where increasing SAA % from 0.5% in F3 to 1.5% in F4 while other factors kept constant reduced EE% from 58.9% to 50.8%, respectively. The same conclusion was observed in both F11 and F13, which contain 0.5% SAA, and their EE% were 61.9% and 71.4%, respectively, while SAA conc increased. to 1.5% reduced the EE% of their corresponding formulas F6 and F12 to 57% and 58.7%, respectively. The other independent variables (X_1 and X_3) also had negative antagonistic main effects on EE% with a *p*-value of 0.0173 and 0.0110, respectively, where individually increasing each variable while keeping other variables unchanged triggered a significant reduction in the encapsulated drug percentage. A comparison of EE% in F2 (77.3%) with that of F14 (55%) demonstrates that adding lecithin in an amount of 100 mg resulted in a significant reduction in EE% while other factors were preserved constant. That result was in line with earlier research [28]. Similarly, the effect of liquid lipid percentage to total lipid was noted in table 2, where increasing liquid lipid concentration from 0 in F2 to 30% in F7 while keeping other factors constant will significantly reduce EE% from 77.3% to 60%, i. e., as the amount of solid lipid (Precirol) increased, the EE% would be found to be higher. This important conclusion could be connected to several factors, firstly; the esterification of glycerol by long-chain fatty acids and the lack of PEG ester in precirol contribute to hydrophobic characteristics to precirol (HLB = 2), which could explain why FLUTAMIDE is encapsulated. Secondly, from the perspective of the chemical structure, precirol is considered an ester of long-chain fatty acids, e. g., palmitic and stearic acids with glycerol, composed of a mixture of mono-, di-, and triglyceride esters (mainly diglyceride), so when it is used to prepare lipid nanoparticles, it provides a highly porous structural matrix with many imperfections that facilitate better drug accommodation, furthermore, as previously mentioned, as the liquid lipid percentage increases, the vesicular size of the produced NLC decreases, and so a smaller space would be available for the accommodation of FLUTAMIDE, which augmented its leakage to the surrounding aqueous medium and therefore decreased the EE%, and finally, the lipid precipitation mechanism that takes place during formula production could be the cause of this. Drug and lipids are mixed together in each droplet; as the formula cools, the lipid precipitates before the drug does, leaving the core either devoid of drug or containing less drug [10, 28, 47, 50]. Besides the main effect of

factors, a significant synergistic interaction X_1X_3 was found to affect the EE%. This interaction couldn't be explained apart from the main effect of factors (X_1 and X_3), for example, in F2 and F14, where at low liquid lipid percentage to total lipid (X_1), increasing the lecithin amount from a low to a high level will significantly reduce the EE% from 77.3% to 55%. This effect is inhibited at high levels of X_1, where the EE% changed slightly from 62.7% in F8 to 60% in F7. The following is the derived polynomial quadratic equation for the EE%:

$$Y_3 = 87.7583-0.889444\ X_1+0.983333\ X_2-0.343333\ X_3-0.00607407\ X_1^2+0.426667\ X_1X_2+0.00833333\ X_1X_3-11.4667\ X_2^2+0.078\ X_2X_3+0.000633333\ X_3^2 .. \text{(Eq. 4)}$$

Preparation of the optimized flutamide-loaded nanocarrier

BBD helped to gain the OF that met our requirements for achieving minimum vesicular size, maximum ζ-potential, and entrapment efficiency. By generating a new formulation based on the anticipated model and assessing the responses as indicated in table 2, the validity of the BBD results was confirmed. The optimal values of the variables were combined to create the OF, which were 29.2% (275.7 Precirol+57.1 mg SPO+57.1 mg PSO), 1.17%, and 100 mg of X_1, X_2, and X_3, respectively, using the hot emulsification ultra-sonication technique, and then characterized as previously stated. The measured values of the responses were compared with the predicted values as follows: the observed response values for Y_1, Y_2, and Y_3 were found to be 330.2 nm,-43.1 mV, and 66.1%, respectively, whereas the predicted values were 268.6 nm,-38.4 mV, and 62.1%, respectively. The observed values were found to fall within a 95% Confidence Interval (C. I) of the predicted values, as depicted in table 2, indicating that the applied design was reasonably valuable for optimizing flutamide-loaded NCs.

Transmission electron microscopy

The morphology and size of the flutamide-containing lipid nanoparticles were examined using a TEM. As revealed in fig. 4A, the optimized formula of BBD shows spherical vesicles with a clear core that looks like oil globules, which may indicate the formation of multiple-type NLC. The drug being entrapped into the oily compartments within the solid lipid is an advantage that enhances the amount of the entrapped drug in this type of NLC. As shown in fig. 4B, the formula WL prepared exactly as OF but without incorporation of liquid oils displays also sphere-shaped vesicles with a nearly clear core that appear to have some darker areas within the core, which may confirm the formation of a nanocarrier with the varied chain lengths of the solid lipid (Precirol) that composed of mixed esters of glycerol (mono-, di-and triglycerides) with both stearic and palmitic acids, a structure that provides many imperfections looks like a wall built from different shaped stones, the huge number of imperfections will leads to increase drug loading capacity as confirmed with observing table 2, where F2 had the highest EE% of all the prepared formulas. Conversely, a solid lipid as stearic acid, which is composed of a single chain of 18 carbons. when used in the prepartion of lipid nanoparticles, the stearic acid chains rearrange into a brick wall-like structure that offers a limited space for entrapping the drug that would be collected into the outer shell and released rapidly into the outer medium, which gives a lower EE% [22, 23].

Physical characterization of flutamide-loaded NCs

Morphological study

The lyophilized formula (OF) was examined using a SEM. Fig. 4C shows that the drug was initially crystalline but eventually became amorphous after being encapsulated into NLCs. Fig. 4D and E showed that the particles were almost spherical or oval, had smooth surfaces, and had diameters that were almost consistent with the Malvern particle size analyzer.
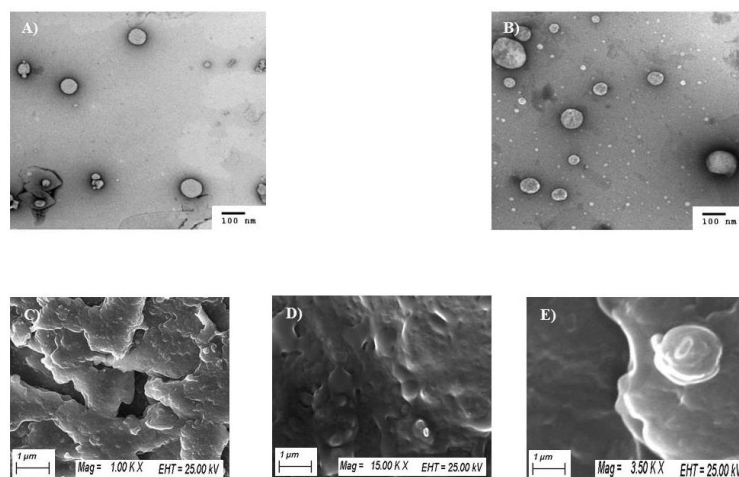

Fig. 4: TEM photomicrographs of the different types of flutamide-loaded lipid nanocarriers. (A) Flutamide-loaded optimized formula, (B) Flutamide-loaded formula without liquid lipid, SEM photomicrograph of flutamide-loaded optimized formula shows (C) The amorphous nature of the formulated NLC, (D), and (E) The spherical topography of the vesicles with their smooth surfaces

Differential scanning calorimetry (DSC)

DSC is considered a thermo-analytical method that is widely used following nanoparticle preparation, including SLNs and NLCs, in order to primarily investigate the solid state of the drug encapsulated within the nanocarrier in comparison with other components included in the formula in order to show the difference between the amorphous and crystalline nature. As depicted in fig. 5A and 5C, pure flutamide and precirol thermograms show sharp endothermic peaks at 111.3 and 60.68 °C, respectively. In contrast, lecithin shows no peak until 160 °C, as shown in fig. 5B. By observing fig. 5E and 5F, we note a reduction of flutamide crystallinity in both OF and WL evidenced by the near disappearance and broadening of the distinctive flutamide endotherm and that the reduction was greater in the OF than WL (prepared using Precirol alone). Also we

note that the addition of liquid lipids to Precirol has led to a shift to lesser temperatures (from 60.68 °C to 58.5 °C) that may be attributed to the interaction of the dispersed oils with Precirol that leads to less order in the structure of the solid lipid matrix that enhance the formation of a less crystalline form than in WL, that finding was in compliance with a previous study that argued the DSC thermograms of flutamide in different lipids including Precirol and also a study that used Biclutamide as the encapsulated drug [22, 45, 52]. Secondly, approve the compatibility by excluding the interactions between different components within the formulation that were evident via observing fig. 5D, which shows the DSC thermogram of the physical mixture of all the components of the formula that reveal the two characteristic peaks of flutamide and Precirol at nearly the same temperatures, 109 and 58 °C, respectively, as temperatures of the individual components.
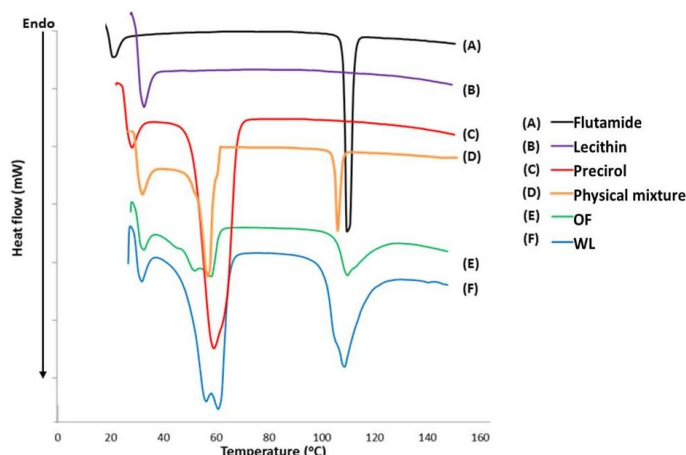
Fig. 5: DSC themograms of: (A) is pure Flutamide, (B) is lecithin, (C) Precirol, (D) is physical mixture of Flutamide, Precirol, and lecithin, (E) Flutamide-loaded optimized formula, and (F) flutamide-loaded formula without liquid lipid

X-ray diffraction (XRD) analysis

The outcomes concluded by DSC analysis were confirmed by powder X-ray diffraction. XRD was also used to study the crystalline nature of flutamide and of flutamide-loaded NCs, where highly crystalline materials produce sharp, high-intensity peaks. In contrast, an amorphous one with a defective lattice produces low-intensity reflections [28]. The chemical properties of the lipids are important for proper drug loading. A greater number of drug molecules can be fit within lipid crystals as precirol, which are combinations of mono-, di-, and triglycerides and contain fatty acids with varying chain lengths [44]. Fig. 6 reveals pure flutamide, OF, and WL X-ray diffractograms. As depicted in fig. 6A, pure flutamide showed characteristic sharp diffraction peaks at 2θ of 8.596°, 17.186°,

18.783°, 23.278°, and 24.877° with some small intensity peaks that corresponded to the crystalline nature of pure flutamide as stated previously [8]. These peaks' intensity has been decreased in both OF and WL, as shown in fig. 6B and 6C, which confirm the phase conversion of flutamide from pure crystalline arrangement to nearly amorphous or molecular dispersion form, while OF shows a lower crystallinity than WL that may be attributed to the presence of liquid lipids that increase the imperfections within the solid lipid lattice, which provides a great space for drug accommodation. The characteristic peak shown at 2θ of 20.842° of both of and WL diffractograms may be attributed to precirol, and it is considered typical for the waxy substances [45]. The reduction of crystallinity after being encapsulated in lipid NCs would probably enhance the solubility of sparingly water-soluble flutamide and its absorption.
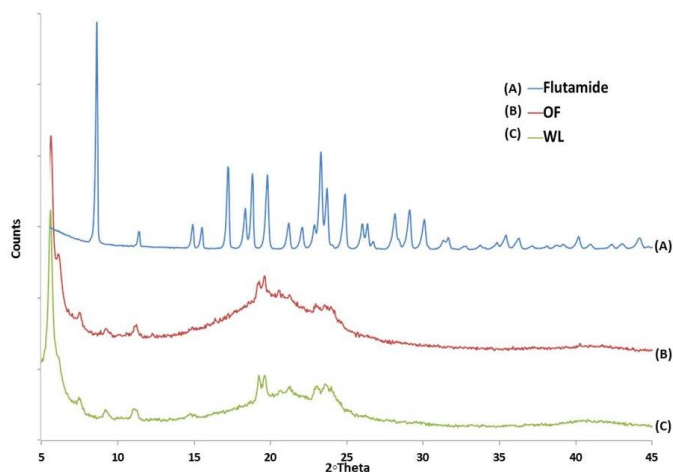

Fig. 6: X-ray diffraction (XRD) where: (A) is pure flutamide, (B) is flutamide-loaded optimized formula, and (C) FLUTAMIDE-loaded formula without liquid lipid

Cytotoxicity assay (MTT assay)

The cytotoxicity of OF was assessed using MTT assays against PC-3 and VERO in comparison with WL and FDS. The outcomes were shown in fig. 7A and table 4, which reveal that the drug-loaded NC (OF) and (WL) IC_{50} were reduced to 3.9±0.05 µg/ml (about 4-fold) and 4.54±0.03 µg/ml (about 3-fold), respectively, compared to 15.02±0.21 µg/ml of FDS on PC-3 that show significance at $P<0.05$. The cytotoxic effect of the sparingly water-soluble flutamide on examined cells (PC-3) appears to be enhanced by its incorporation into the lipid carrier, which enhances the drug's ability to enter the cells through mechanisms like endocytosis [52]. Compared to un-entrapped drugs,

nanocarriers offer numerous benefits, including resistance against degradation, enhanced and directed uptake into the intended tissue, and control over the pharmacokinetics and distribution of the drug to tissue. These results were consistent with earlier research on various nanoparticles, including NLCs, which showed that NLC entrapment could increase the drug's effectiveness and reduce the amount of drug needed to be used, thus improving safety [53–58]. Another important finding was that the IC_{50} of OF was 3.9±0.05 µg/ml, which was reduced about one-fold compared to 4.54±0.03 µg/ml of WL. This reduction was significant at $P<0.05$, which may indicate the additive effect of the liquid oils used (SPO and PSO) with flutamide enhancing the inhibitory effect of OF over WL. Regarding safety for the normal cells, the

cytotoxic effects of OF, WL, and FDS were assessed on the VERO normal cells over a matching concentration range from 0.01-100 μg/ml, where all had harmless effects on the VERO normal cells with concentrations greater than 100 μg/ml, as illustrated in fig. 7B. This demonstrates the drug's specificity towards cancer cells while posing little risk to healthy cells.

Table 4: IC$_{50}$ of optimized formula, formula without liquid lipids, and free flutamide suspension

Formula	Component (s)					IC$_{50}$ (μg/ml)	
	Precirol 70.8%	PSO+SPO 29.2%	Lecithin 100 mg	Tween 20 1.17%	Flutamide 10 mg	PC-3*	VERO
OF	✓	✓	✓	✓	✓	3.90*±0.05	>100
WL	✓	-	✓	✓	✓	4.54*±0.03	>100
FDS	Free Flutamide suspension					15.02*±0.21	>100

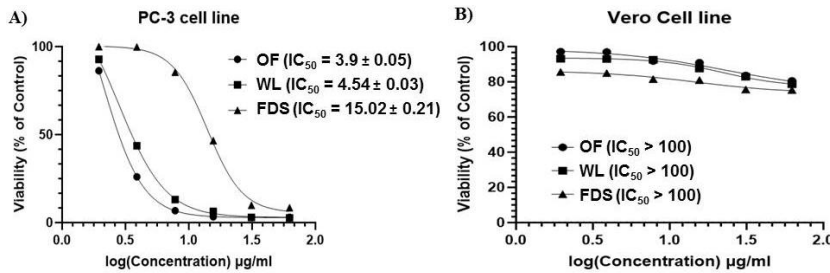Note: *donates significance differenece at a *P*-value<0.05. *Results presented as mean±SD

Fig. 7: Cytotoxicity assay against (A) prostate cancer cell line (PC-3), and (B) normal hamster kidney cell line (VERO), Results presented as mean

***In vivo* pharmacokinetic study of the optimized formula on male rats**

After oral single-dose administration of OF, WL, and FDS to male rats, the calculated pharmacokinetic parameters and the mean plasma concentration-time curves of flutamide were shown in table 5 and fig. 8, respectively. Oral bioavailability was greatly enhanced when flutamide was administered as a nanocarrier, as demonstrated by the obtained pharmacokinetic parameters. For instance, the flutamide-loaded OF and WL maximum plasma concentration (C$_{max}$) was found to be 559.35±41.79 ng/ml and 670.9±24.61 ng/ml, respectively, which is considered 2-fold higher than the C$_{max}$ of FDS (281.4±94.33 ng/ml) with a *p*-value<0.05. While the C$_{max}$ of both OF and WL showed no statistically significance difference at the same *p*-value, the C$_{max}$ of WL was a little bit higher than the C$_{max}$ of OF. This increase can be attributed to the increased rate of flutamide release from the oil-containing NLC formulation, which breaks down the unentrapped drug before it can be absorbed. Additionally, precirol in OF is partially replaced with the two oils, which may be connected to this as prior research has demonstrated that long-chain fatty acid triglycerides perform well during lymphatic absorption [59]. Also, the AUC$_{0-\infty}$ was increased 1.5–2 times in both OF (143498.69±35198.67 ng/ml x min^2) and WL (174331.06±34435.68 ng/ml x min^2) in comparison with that of FDS (85180.55±9395.19 ng/ml x min^2) with *p*-value<0.1. The previous findings could be explained by the transportation of nanocarrier contents to intestinal cells by vesicular endocytosis; additionally, the lymphatic system's ability to transport FLUTAMIDE-loaded NCs could be another plausible explanation for avoiding the initial hepatic metabolism, which has a significant impact on free flutamide [60].
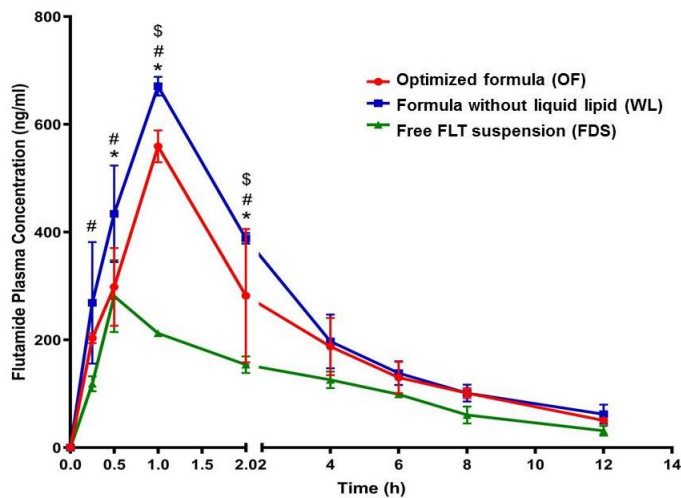

Fig. 8: Plasma concentration-time curve of Flutamide (flutamide) after single oral administration of 26 mg/kg of flutamide-loaded optimized formula, flutamide-loaded formula without liquid lipid, and free flutamide suspension, Note: # Significant difference between WL vs FDS at *P*<0.05, * Significant difference between WL and OF at *P*<0.05, and $ Significant difference between OF vs FDS. Results presented as mean±SD

Table 5: Pharmacokinetic parameters after oral administration of a single dose (26 mg/kg) of the OF, WL in comparison with FDS

Pharmacokinetic parameter	OF	WL	FDS
$t_{1/2}$ (min)	288.44±67.90	312.59±76.32	249.86±60.81
C_{max} (ng/ml)	559.35±41.79*	670.9±24.61*	281.4±94.33
$AUC_{(0-720)}$ (ng/ml x min)	122781.97±36928.26	144928.72±16335.54	73246.12±2013.66
$AUC_{(720-\infty)}$ (ng/ml x min)	20716.72±1729.59	29402.34±18100.14	11934.43±7381.53
$AUC_{(0-\infty)}$ (ng/ml x min)	143498.69±35198.67	174331.06±34435.68	85180.55±9395.19
$AUMC_{(0-\infty)}$ (ng/ml x min^2)	52588857.52#±3800040.81	67563903.95#±31981704.98	31546768.17±10915969.75
$MRT_{(0-\infty)}$ (min)	374.49±65.38	376.79± 109.02	365.51±87.84

Note: *significantly differs from values of FDS at a *P*-value<0.05, while #significantly differs from values of FDS at a *P*-value<0.1, Results presented as mean±SD

CONCLUSION

Lipid nanocarriers, as an auspicious drug delivery system, are used to efficiently incorporate the sparingly water-soluble flutamide within their core, which reduces its crystallinity, increasing water solubility and consequently its oral bioavailability. The BBD was applied to optimize the vesicular size (330.2 nm), zeta potential (-43.1 mV), and EE% (66.1%) of the optimized flutamide-loaded nanocarrier by selecting liquid lipid percentage to total lipids at 29.2%, lecithin at 100 mg, and tween 20 % at 1.17%. The optimized flutamide-loaded nanocarrier (OF) and its corresponding formula (WL) show great selectivity toward PC-3 cells with IC_{50} of 3.90±0.05 μg/ml and 4.54±0.03 μg/ml, respectively, without affecting healthy cells with IC_{50}>100 μg/ml. Also the addition of both SPO and PSO together with flutamide give a significantly additive effect than flutamide alone against PC-3 cell line. Moreover, the enhancement in bioavailability of both OF and WL with a C_{max} of 559.35±41.79 ng/ml and 670.9±24.61 ng/ml, respectively, can be applied in the future to decrease the total daily dose of flutamide and so lessen its associated side effects. The lipid nanoparticle technique can also be applied to other drugs belonging to BCS class II to enhance their pharmacokinetic and pharmacodynamic properties.

ACKNOWLEDGMENT

FUNDING

AUTHORS CONTRIBUTIONS

All authors contributed to the study conception and design, material preparation, data collection, and analysis.

CONFLICT OF INTERESTS

The authors declare that they have no competing interests.

REFERENCES

1. Blair HA. Hexanic extract of serenoa repens (Permixon®): a review in symptomatic benign prostatic hyperplasia. Drugs Aging. 2022;39(3):235-43. doi: 10.1007/s40266-022-00924-3, PMID 35237936.
2. leisegang K, Jimenez M, Durairajanayagam D, Finelli R, Majzoub A, Henkel R. Phytomedicine plus a systematic review of herbal medicine in the clinical treatment of benign prostatic hyperplasia. Phytomedicine Plus. 2022;2(1):100-53. doi: 10.1016/j.phyplu.2021.100153.
3. Ali MA, Mohamed MI, Megahed MA, Abdelghany TM, El-Say KM. Cholesterol-based nanovesicles enhance the *in vitro* cytotoxicity, ex vivo intestinal absorption, and *in vivo* bioavailability of flutamide. Pharmaceutics. 2021;13(11):1-22. doi: 10.3390/pharmaceutics13111741, PMID 34834155.
4. Giorgetti R, di Muzio M, Giorgetti A, Girolami D, Borgia L, Tagliabracci A. Flutamide-induced hepatotoxicity: ethical and scientific issues. Eur Rev Med Pharmacol Sci. 2017;21(1)Suppl:69-77. PMID 28379593.
5. Khan N, Abdelhamid HN, Yan JY, Chung FT, Wu HF. Detection of flutamide in pharmaceutical dosage using higher electrospray ionization mass spectrometry (ESI-MS) tandem mass coupled with Soxhlet apparatus. Anal Chem Res. 2015;3(Feb):89-97. doi: 10.1016/j.ancr.2015.01.001.
6. Rojas PA, Iglesias TG, Barrera F, Mendez GP, Torres J, San Francisco IF. Acute liver failure and liver transplantation secondary to flutamide treatment in a prostate cancer patient. Urol Case Rep. 2020;33:101370. doi: 10.1016/j.eucr.2020.101370, PMID 33102069.
7. Jeevana JB, Sreelakshmi K. Design and evaluation of self-nanoemulsifying drug delivery system of flutamide. J Young Pharm. 2011;3(1):4-8. doi: 10.4103/0975-1483.76413, PMID 21607048.
8. Elgindy N, Elkhodairy K, Molokhia A, Elzoghby A. Lyophilization monophase solution technique for improvement of the physicochemical properties of an anticancer drug, flutamide. Eur J Pharm Biopharm. 2010;74(2):397-405. doi: 10.1016/j.ejpb.2009.11.011, PMID 19944160.
9. Youssef SF, Elnaggar YS, Abdallah OY. Elaboration of polymersomes versus conventional liposomes for improving oral bioavailability of the anticancer flutamide. Nanomedicine (Lond). 2018;13(23):3025-36. doi: 10.2217/nnm-2018-0238, PMID 30507344.
10. Bakhaidar RB, Hosny KM, Mahier IM, Rizq WY, Safhi AY, Bukhary DM. Development and optimization of a tamsulosin nanostructured lipid carrier loaded with saw palmetto oil and pumpkin seed oil for treatment of benign prostatic hyperplasia. Drug Deliv. 2022;29(1):2579-91. doi: 10.1080/10717544.2022.2105448, PMID 35915055.
11. Andjelkovic M, Van Camp J, Trawka A, Verhe R. Phenolic compounds and some quality parameters of pumpkin seed oil. Euro J Lipid Sci & Tech. 2010;112(2):208-17. doi: 10.1002/ejlt.200900021.
12. Alhakamy NA, Fahmy UA, Ahmed OA. Attenuation of benign prostatic hyperplasia by optimized tadalafil loaded pumpkin seed oil-based self nanoemulsion: *in vitro* and *in vivo* evaluation. Pharmaceutics. 2019;11(12):1-13. doi: 10.3390/pharmaceutics11120640, PMID 31805693.
13. Csikos E, Horvath A, Acs K, Papp N, Balazs VL, Dolenc MS. Treatment of benign prostatic hyperplasia by natural drugs. Molecules. 2021;26(23):1-32. doi: 10.3390/molecules26237141, PMID 34885733.
14. Anastassakis K. Androgenetic alopecia from A to Z. 1st ed. Vol. 2, Androgenetic Alopecia From A to Z. Springer Cham; 2022. p. 193-7.
15. Kalwat JI. The use of serenoa repens (saw palmetto) in hair care products. BJSTR. 2019;13(1):9725-8. doi: 10.26717/BJSTR.2019.13.002348.
16. Zhang Y, Zhang P, Zhu T. Ovarian carcinoma biological nanotherapy: comparison of the advantages and drawbacks of lipid, polymeric, and hybrid nanoparticles for cisplatin delivery. Biomed Pharmacother. 2019;109(1):475-83. doi: 10.1016/j.biopha.2018.10.158, PMID 30399584.
17. Davis ME, Chen ZG, Shin DM. Nanoparticle therapeutics: an emerging treatment modality for cancer. Nat Rev Drug Discov. 2008;7(9):771-82. doi: 10.1038/nrd2614, PMID 18758474.
18. Xin Y, Huang Q, Tang JQ, Hou XY, Zhang P, Zhang LZ. Nanoscale drug delivery for targeted chemotherapy. Cancer Lett. 2016;379(1):24-31. doi: 10.1016/j.canlet.2016.05.023, PMID 27235607.

19. Nguyen CN, Nguyen TT, Nguyen HT, Tran TH. Nanostructured lipid carriers to enhance transdermal delivery and efficacy of diclofenac. Drug Deliv Transl Res. 2017;7(5):664-73. doi: 10.1007/s13346-017-0415-2, PMID 28776220.

20. Carbone C, Campisi A, Musumeci T, Raciti G, Bonfanti R, Puglisi G. FA-loaded lipid drug delivery systems: preparation, characterization and biological studies. Eur J Pharm Sci. 2014;52(1):12-20. doi: 10.1016/j.ejps.2013.10.003, PMID 24514450.

21. Vidlarova L, Hanus J, Vesely M, Ulbrich P, Stepanek F, Zbytovska J. Effect of lipid nanoparticle formulations on skin delivery of a lipophilic substance. Eur J Pharm Biopharm. 2016;108:289-96. doi: 10.1016/j.ejpb.2016.07.016, PMID 27449632.

22. Muller RH, Radtke M, Wissing SA. Nanostructured lipid matrices for improved microencapsulation of drugs. Int J Pharm. 2002;242(1-2):121-8. doi: 10.1016/s0378-5173(02)00180-1, PMID 12176234.

23. Üner M. Preparation, characterization and physico-chemical properties of solid lipid nanoparticles (SLN) and nanostructured lipid carriers (NLC): their benefits as colloidal drug carrier systems. Pharmazie. 2006;61(5):375-86. PMID 16724531.

24. Aslam R, Tiwari V, Upadhyay P, Tiwari A. Original article revolutionizing therapeutic delivery: diosgenin-loaded solid lipid nanoparticles unleash advanced carriers. International Journal of Applied Pharmaceutics. 2024;16(1):124–33. doi: 10.22159/ijap.2024v16i1.49306.

25. lópez KL, Ravasio A, Gonzalez Aramundiz JV, Zacconi FC. Solid lipid nanoparticles (SLN) and nanostructured lipid carriers (NLC) prepared by microwave and ultrasound-assisted synthesis: promising green strategies for the nanoworld. Pharmaceutics. 2023;15(5):1-26. doi: 10.3390/pharmaceutics15051333, PMID 37242575.

26. El-Say KM, Hosny KM. Optimization of carvedilol solid lipid nanoparticles: an approach to control the release and enhance the oral bioavailability on rabbits. PLOS ONE. 2018;13(8):e0203405. doi: 10.1371/journal.pone.0203405, PMID 30161251.

27. El-Say KM, El-Helw AR, Ahmed OA, Hosny KM, Ahmed TA, Kharshoum RM. Statistical optimization of controlled release microspheres containing cetirizine hydrochloride as a model for water-soluble drugs. Pharm Dev Technol. 2015;20(6):738-46. doi: 10.3109/10837450.2014.920353, PMID 24856961.

28. Kudarha R, Dhas NL, Pandey A, Belgamwar VS, Ige PP. Box-behnken study design for optimization of bicalutamide-loaded nanostructured lipid carrier: stability assessment. Pharm Dev Technol. 2015;20(5):608-18. doi: 10.3109/10837450.2014.908305, PMID 24785784.

29. Ferreira N, Viana T, Henriques B, Tavares DS, Jacinto J, Colonia J. Application of response surface methodology and box-behnken design for the optimization of mercury removal by Ulva sp J Hazard Mater. 2023;445:130405. doi: 10.1016/j.jhazmat.2022.130405, PMID 36437192.

30. Aodah AH, Hashmi S, Akhtar N, Ullah Z, Zafar A, Zaki RM. Formulation development, optimization by box-behnken design, and *in vitro* and ex vivo characterization of hexatriacontane-loaded transethosomal gel for antimicrobial treatment for skin infections. Gels. 2023;9(4):1-22. doi: 10.3390/gels9040322, PMID 37102934.

31. Patra S. Development, characterization and pharmacokinetic evaluation of optimized vildagliptin sustained release matrix tablet using box-behnken design. International Journal of Applied Pharmaceutics. 2024;16(1):214-23. doi: 10.22159/ijap.2024v16i1.48052.

32. Hosny KM, Aljaeid BM. Sildenafil citrate as oral solid lipid nanoparticles: a novel formula with higher bioavailability and sustained action for treatment of erectile dysfunction. Expert Opin Drug Deliv. 2014;11(7):1015-22. doi: 10.1517/17425247.2014.912212, PMID 24746063.

33. Li Y, Zhao X, Zu Y, Zhang Y. Preparation and characterization of paclitaxel nanosuspension using novel emulsification method by combining high speed homogenizer and high pressure homogenization. Int J Pharm. 2015;490(1-2):324-33. doi: 10.1016/j.ijpharm.2015.05.070, PMID 26027492.

34. Ahmed TA, El-Say KM, Aljaeid BM, Fahmy UA, Abd-Allah FI. Transdermal glimepiride delivery system based on optimized

ethosomal nano-vesicles: Preparation, characterization, *in vitro*, ex vivo and clinical evaluation. Int J Pharm. 2016;500(1-2):245-54. doi: 10.1016/j.ijpharm.2016.01.017, PMID 26775063.

35. Manconi M, Sinico C, Valenti D, lai F, Fadda AM. Niosomes as carriers for tretinoin. III. A study into the *in vitro* cutaneous delivery of vesicle-incorporated tretinoin. Int J Pharm. 2006;311(1-2):11-9. doi: 10.1016/j.ijpharm.2005.11.045, PMID 16439071.

36. El-Ridy MS, Abd ElRahman AA, Awad GM, Khalil RM, Younis MM. *In vitro* and *in vivo* evaluation of niosomes containing celecoxib. IJPSR. 2014;5(11):4677-88. doi: 10.13040/IJPSR.0975-8232.5(11).4677-88.

37. Elzoghby AO, Helmy MW, Samy WM, Elgindy NA. Novel ionically crosslinked casein nanoparticles for flutamide delivery: formulation, characterization, and *in vivo* pharmacokinetics. Int J Nanomedicine. 2013;8:1721-32. doi: 10.2147/IJN.S40674, PMID 23658490.

38. Mosmann T. Rapid colorimetric assay for cellular growth and survival: application to proliferation and cytotoxicity assays. J Immunol Methods. 1983;65(1-2):55-63. doi: 10.1016/0022-1759(83)90303-4, PMID 6606682.

39. Scudiero DA, Shoemaker RH, Paull KD, Monks A, Tierney S, Nofziger TH. Evaluation of a soluble tetrazolium/formazan assay for cell growth and drug sensitivity in culture using human and other tumor cell lines. Cancer Res. 1988;48(17):4827-33. PMID 3409223.

40. Elzoghby AO, Helmy MW, Samy WM, Elgindy NA. Spray-dried casein-based micelles as a vehicle for solubilization and controlled delivery of flutamide: formulation, characterization, and *in vivo* pharmacokinetics. Eur J Pharm Biopharm. 2013;84(3):487-96. doi: 10.1016/j.ejpb.2013.01.005, PMID 23403015.

41. Khames A, Khaleel MA, El-Badawy MF, El-Nezhawy AO. Natamycin solid lipid nanoparticles-sustained ocular delivery system of higher corneal penetration against deep fungal keratitis: preparation and optimization. Int J Nanomedicine. 2019;14:2515-31. doi: 10.2147/IJN.S190502, PMID 31040672.

42. Madhusudhan B, Rambhau D, Apte SS, Gopinath D. Oral bioavailability of flutamide from 1-o-alkylglycerol stabilized o/w nanoemulsions. J Dispers Sci Technol. 2007;28(8):1254-61. doi: 10.1080/01932690701528241.

43. Chalikwar SS, Belgamwar VS, Talele VR, Surana SJ, Patil MU. Formulation and evaluation of nimodipine-loaded solid lipid nanoparticles delivered via lymphatic transport system. Colloids Surf B Biointerfaces. 2012;97:109-16. doi: 10.1016/j.colsurfb.2012.04.027, PMID 22609590.

44. Araujo J, Gonzalez Mira E, Egea MA, Garcia ML, Souto EB. Optimization and physicochemical characterization of a triamcinolone acetonide-loaded NLC for ocular antiangiogenic applications. Int J Pharm. 2010;393(1-2):167-75. doi: 10.1016/j.ijpharm.2010.03.034, PMID 20362042.

45. Kumbhar DD, Pokharkar VB. Engineering of a nanostructured lipid carrier for the poorly water-soluble drug, bicalutamide: physicochemical investigations. Colloids and Surfaces A: Physicochemical and Engineering Aspects. 2013;416:32-42. doi: 10.1016/j.colsurfa.2012.10.031.

46. Walbi IA, Ahmad MZ, Ahmad J, Algahtani MS, Alali AS, Alsudir SA. Development of a curcumin-loaded lecithin/chitosan nanoparticle utilizing a box-behnken design of experiment: formulation design and influence of process parameters. Polymers (Basel). 2022;14(18):1-17. doi: 10.3390/polym14183758, PMID 36145903.

47. Agrawal Y, Petkar KC, Sawant KK. Development, evaluation and clinical studies of acitretin-loaded nanostructured lipid carriers for topical treatment of psoriasis. Int J Pharm. 2010;401(1-2):93-102. doi: 10.1016/j.ijpharm.2010.09.007, PMID 20858539.

48. WC. Ageing effects in parenteral fat emulsions: the role of fatty acids. International Journal of Pharmaceutics. 1987;39:33-7.

49. Chinsriwongkul A, Chareanputtakhun P, Ngawhirunpat T, Rojanarata T, Sila-on W, Ruktanonchai U. Nanostructured lipid carriers (NLC) for parenteral delivery of an anticancer drug. AAPS PharmSciTech. 2012;13(1):150-8. doi: 10.1208/s12249-011-9733-8, PMID 22167418.

50. Guada M, Sebastian V, Irusta S, Feijoo E, Dios Vieitez Mdel C, Blanco Prieto MJ. Lipid nanoparticles for cyclosporine a administration: development, characterization, and *in vitro* evaluation of their immunosuppression activity. Int J Nanomedicine. 2015;10:6541-53. doi: 10.2147/IJN.S90849, PMID 26527872.

51. Aboud HM, El Komy MH, Ali AA, El Menshawe SF, Abd Elbary A. Development, optimization, and evaluation of carvedilol-loaded solid lipid nanoparticles for intranasal drug delivery. AAPS PharmSciTech. 2016;17(6):1353-65. doi: 10.1208/s12249-015-0440-8, PMID 26743643.

52. Bondì ML, Craparo EF, Giammona G, Cervello M, Azzolina A, Diana P. Nanostructured lipid carriers-containing anticancer compounds: preparation, characterization, and cytotoxicity studies. Drug Deliv. 2007;14(2):61-7. doi: 10.1080/10717540600739914, PMID 17364869.

53. Chandratre SS, Dash AK. Multifunctional nanoparticles for prostate cancer therapy. AAPS PharmSciTech. 2015;16(1):98-107. doi: 10.1208/s12249-014-0202-z, PMID 25190362.

54. Mortazavi SM, Mohammadabadi MR, Khosravi Darani K, Mozafari MR. Preparation of liposomal gene therapy vectors by a scalable method without using volatile solvents or detergents. J Biotechnol. 2007;129(4):604-13. doi: 10.1016/j.jbiotec.2007.02.005, PMID 17353061.

55. Shenoy VS, Gude RP, Murthy RS. *In vitro* anticancer evaluation of 5-fluorouracil lipid nanoparticles using B16F10 melanoma cell lines. Int Nano Lett. 2013;3(1):36. doi: 10.1186/2228-5326-3-36.

56. Tavano L, Aiello R, Ioele G, Picci N, Muzzalupo R. Niosomes from glucuronic acid-based surfactant as new carriers for cancer therapy: preparation, characterization and biological properties. Colloids Surf B Biointerfaces. 2014;118:7-13. doi: 10.1016/j.colsurfb.2014.03.016, PMID 24709252.

57. Danhier F, lecouturier N, Vroman B, Jerome C, Marchand Brynaert J, Feron O. Paclitaxel-loaded pegylated PLGA-based nanoparticles: *in vitro* and *in vivo* evaluation. J Control Release. 2009;133(1):11-7. doi: 10.1016/j.jconrel.2008.09.086, PMID 18950666.

58. Sharma V, Anandhakumar S, Sasidharan M. Self-degrading niosomes for encapsulation of hydrophilic and hydrophobic drugs: an efficient carrier for cancer multi-drug delivery. Mater Sci Eng C Mater Biol Appl. 2015 Nov;56:393-400. doi: 10.1016/j.msec.2015.06.049, PMID 26249606.

59. Dolatabadi S, Karimi M, Nasirizadeh S, Hatamipour M, Golmohammadzadeh S, Jaafari MR. Preparation, characterization and in vivo pharmacokinetic evaluation of curcuminoids-loaded solid lipid nanoparticles (SLNs) and nanostructured lipid carriers (NLCs). J Drug Deliv Sci Technol. 2021;62:102352. doi: 10.1016/j.jddst.2021.102352.

60. Veerareddy PR, Bobbala SK. Enhanced oral bioavailability of isradipine via proniosomal systems. Drug Dev Ind Pharm. 2013;39(6):909-17. doi: 10.3109/03639045.2012.717945, PMID 22998221.